Preprint typeset in JHEP style - HYPER VERSION

Photon-radion conversion cross-sections in external electromagnetic field

P. V. Dong[a], **H. N. Long**[a], **D. V. Soa**[b] **and N. H.Thao**[a]

[a] *Institute of Physics, VAST, 10 Dao Tan, Ba Dinh, Hanoi, Vietnam*
[b] *Department of Physics, Hanoi University of Education, Hanoi, Vietnam*
E-mail: pvdong@iop.vast.ac.vn, hnlong@iop.vast.ac.vn, dvsoa@assoc.iop.vast.ac.vn, nhthao@grad.iop.vast.ac.vn

Abstract: An attempt is made to present some experimental predictions of the Randall-Sundrum model, where compactification radius of the extra dimension is stabilized by the radion, which is a scalar field lighter than the graviton Kaluza-Klein states. We calculate the conversion cross-sections of the photons into the radions in the external electromagnetic fields, namely, in the static fields and in a periodic field of the wave guide. Numerical evaluations of the total cross-sections are also given. Our result shows that the conversion cross-section in the static electric field is quite small. But, in the static magnetic and periodic fields, the radion productions are much enhanced.

Keywords: Radion, Randall-Sundrum model.

Contents

1. Introduction

There has been a lot attention devoted to the models of physics above the weak scale utilizing extradimensions in solving the hierarchy problem. Firstly, Arkani-Hamed, Dimopoulos and Dvali [1] have suggested that the fundamental scale of quantum gravity could be dramatically much lower than the Planck scale provided the standard model (SM) fields propagate on a 3-dimensional brane and the gravity propagates in extraspace dimensions. The smallness of Newton's constant can then be explained by the large size of the volume of compactification. An alternative approach as proposed by Randall and Sundrum (RS) [2] can also solve the hierarchy problem by localizing all the SM particles on the visible brane or TeV brane of a non-factorizable geometry like a slice of five-dimensional (5D) anti de-Sitter space with curvature κ. The fifth dimension of this space is S^1/Z_2 orbifold of size r labeled by a coordinate $y \in [0, 1/2]$, such that the points (x^μ, y) and $(x^\mu, -y)$ are identified. The four-dimensional (4D) massless graviton field is localized on another brane away from our brane. Since the fundamental gravity scales as motivated by the hierarchy problem were not much bigger than a TeV, these scenarios would have distinctive signatures in collider experiments.

In the RS model the compactification radius is in the order of Planck length and interestingly is a dynamical object. It is connected to the vacuum expectation value (VEV) of the dilaton field arising due to the compactification of full 5D theory to 4D. The radion field is an exponential function of the dilaton field scaled by proper factors [3]. Much research has been done on understanding a possible mechanism for radius stabilization and the phenomenology of the radion field in the model [4]. The motivation for studying the radion is twofold. Firstly, the radion may turn out to be the lightest new particle

in the RS-type setup, possibly accessible at the LHC. In addition, the phenomenological similarity and potential mixing of the radion and Higgs boson warrant detailed study in order to facilitate distinction between the radion and Higgs signals at colliders.

One of the intriguing features of the RS models is that the neutral scalar bosons can have interactions with the photon. This feature has been recently investigated in a series of works [5, 6, 7, 8, 9, 10, 11, 12]. The couplings of two photons with neutral scalar bosons provide interesting possibility to search the latter in the external electromagnetic (EM) fields. The light particles with a two photon interaction may be created by a photon entering the EM field, an effect firstly discussed by Primakoff [13]. This effect is the basis of Sikivie's methods for the detection of axions and other light particles in a resonant cavity [14]. The pseudoscalar–photon mixing phenomenon in background magnetic field has been analyzed in detail in the literature [15]. This phenomenon has also been used to impose stringent limits on the pseudoscalar–photon coupling [16]. In the previous works, we have considered the creation of gravitons and dilations [17, 18] and axions [19] in the external EM field.

The aim of this work is to study the phenomenology of radion in the RS model and the conversion possibility of photon into radion in the external EM fields. In contradiction with the previous experiments of gravitons, dilations and axions, the radion in the RS model may be much heavier. Therefore, we should take into account the provided source of high energy photons. One way to achieve the high energy photons is to use the laser backscattering technique [20]. Then the light radion (in order of a few GeV) of the RS model can be produced.

The organization of this paper is follows. In Sec. 2 we give a review of the RS model. In Sec. 3 we present the coupling of radion to photons. Section 4 is devoted to photon-radion conversions in the external EM fields. Namely, we first account for the production of radions in an 100 KV/m external electric field of flat condenser and the case in a 9 Tesla external magnetic field of solenoid in CAST experiments [21]. We next consider the conversion in a periodic EM field of wave guide. Finally, we summarize our results and make conclusions in the last section–Sec. 5.

2. A review of RS model

The RS model is based on a 5D spacetime with non-factorizable geometry [2]. The single extradimension is compactified on a S^1/Z_2 orbifold of which two fixed points accommodate two three-branes (4D hyper-surfaces), the Planck brane at $y = 0$ and TeV brane at $y = 1/2$. The ordinary 4D Poincare invariance is shown to be maintained by the following classical solution to the Einstein equation:

$$ds^2 = e^{-2\sigma(y)}\eta_{\mu\nu}dx^\mu dx^\nu - b_0^2 dy^2, \quad \sigma(y) = m_0 b_0 |y|, \tag{2.1}$$

where x^μ ($\mu = 0, 1, 2, 3$) denote the coordinates on the 4D hyper-surfaces of constant y with metric $\eta_{\mu\nu} = \mathrm{diag}(1, -1, -1, -1)$. The m_0 and b_0 are the fundamental mass parameter and compactification radius, respectively.

Gravitational fluctuations about the RS metric,

$$\eta_{\mu\nu} \to g_{\mu\nu} = \eta_{\mu\nu} + \epsilon h_{\mu\nu}(x,y), \quad b_0 \to b_0 + b(x), \tag{2.2}$$

yield two kinds of new phenomenological ingredients on the TeV brane: the KK graviton modes $h^{(n)}_{\mu\nu}(x)$ and the canonically normalized radion field $\phi_0(x)$, respectively defined as

$$h_{\mu\nu}(x,y) = \sum_{n=0}^{\infty} h^{(n)}_{\mu\nu}(x)\frac{\chi^{(n)}(y)}{\sqrt{b_0}}, \quad \phi_0(x) = \sqrt{6}M_{\rm Pl}\Omega_b(x), \tag{2.3}$$

where $\Omega_b(x) \equiv e^{-m_0[b_0+b(x)]/2}$. The 5D Planck mass M_5 ($\epsilon^2 = 16\pi G_5 = 1/M_5^3$) is related to its 4D one ($M_{\rm Pl} \equiv 1/\sqrt{8\pi G_{\rm N}}$) by

$$\frac{M_{\rm Pl}^2}{2} = \frac{1-\Omega_0^2}{\epsilon^2 m_0}. \tag{2.4}$$

Here $\Omega_0 \equiv e^{-m_0 b_0/2}$ is known as the warp factor. Because our TeV brane is arranged to be at $y = 1/2$, a canonically normalized scalar field has the mass multiplied by the warp factor, i.e, $m_{\rm phys} = \Omega_0 m_0$. Since the moderate value of $m_0 b_0/2 \simeq 35$ can generate TeV scale physical mass, the gauge hierarchy problem is explained.

The 4D effective Lagrangian is then

$$\mathcal{L} = -\frac{\phi_0}{\Lambda_\phi}T^\mu_\mu - \frac{1}{\hat{\Lambda}_W}T^{\mu\nu}(x)\sum_{n=1}^{\infty} h^{(n)}_{\mu\nu}(x), \tag{2.5}$$

where $\Lambda_\phi \equiv \sqrt{6}M_{\rm Pl}\Omega_0$ is the VEV of the radion field, and $\hat{\Lambda}_W \equiv \sqrt{2}M_{\rm Pl}\Omega_0$. The $T^{\mu\nu}$ is the energy-momentum tensor of the TeV brane localized SM fields. The T^μ_μ is the trace of the energy-momentum tensor, which is given at the tree level as [22, 23]

$$T^\mu_\mu = \sum_f m_f \bar{f}f - 2m_W^2 W^+_\mu W^{-\mu} - m_Z^2 Z_\mu Z^\mu + (2m_{h_0}^2 h_0^2 - \partial_\mu h_0 \partial^\mu h_0) + \cdots \tag{2.6}$$

The gravity-scalar mixing arises at the TeV-brane by [6, 7, 8]

$$S_\xi = -\xi \int d^4x\sqrt{-g_{\rm vis}}R(g_{\rm vis})\hat{H}^\dagger\hat{H}, \tag{2.7}$$

where $R(g_{\rm vis})$ is the Ricci scalar for the induced metric on the visible brane or TeV brane, $g^{\mu\nu}_{\rm vis} = \Omega_b^2(x)(\eta^{\mu\nu} + \epsilon h^{\mu\nu})$. $\hat{H}$ is the Higgs field before re-scaling, i.e., $H_0 = \Omega_0\hat{H}$. The parameter ξ denotes the size of the mixing term. With $\xi \neq 0$, there is neither a pure Higgs boson nor pure radion mass eigenstate. This ξ term mixes the h_0 and ϕ_0 fields into the mass eigenstates h and ϕ as given by [7, 8]

$$\begin{pmatrix} h_0 \\ \phi_0 \end{pmatrix} = \begin{pmatrix} 1 & -6\xi\gamma/Z \\ 0 & 1/Z \end{pmatrix}\begin{pmatrix} \cos\theta & \sin\theta \\ -\sin\theta & \cos\theta \end{pmatrix}\begin{pmatrix} h \\ \phi \end{pmatrix} = \begin{pmatrix} d & c \\ b & a \end{pmatrix}\begin{pmatrix} h \\ \phi \end{pmatrix}, \tag{2.8}$$

where

$$\begin{aligned} &\gamma \equiv v_0/\Lambda_\phi, \quad Z^2 \equiv 1 - 6\xi\gamma^2(1+6\xi) = \beta - 36\xi^2\gamma^2, \quad \beta \equiv 1 - 6\xi\gamma^2, \\ &a \equiv \frac{\cos\theta}{Z}, \quad b \equiv -\frac{\sin\theta}{Z}, \quad c \equiv \sin\theta - \frac{6\xi\gamma}{Z}\cos\theta, \quad d \equiv \cos\theta + \frac{6\xi\gamma}{Z}\sin\theta. \end{aligned} \tag{2.9}$$

The mixing angle θ is defined by

$$\tan 2\theta = 12\gamma\xi Z \frac{m_{h_0}^2}{m_{h_0}^2(Z^2 - 36\xi^2\gamma^2) - m_{\phi_0}^2}. \tag{2.10}$$

The new fields h and ϕ are mass eigenstates with masses

$$m_{h,\phi}^2 = \frac{1}{2Z^2}\left[m_{\phi_0}^2 + \beta m_{h_0}^2 \pm \sqrt{(m_{\phi_0}^2 + \beta m_{h_0}^2)^2 - 4Z^2 m_{\phi_0}^2 m_{h_0}^2}\right]. \tag{2.11}$$

The mixing between the states enable decays of the heavier eigenstate into the lighter eigenstates if kinematically allowed. Overall, the production cross-sections, widths and relative branching fractions can all be affected significantly by the value of the mixing parameter ξ [6, 8, 23, 24]. There are also two algebraic constraints on the value of ξ. One comes from the requirement that the roots of the inverse functions of Eq. (2.11) are definitely positive. Suggesting that the Higgs boson is heavier, we get

$$\frac{m_h^2}{m_\phi^2} > 1 + \frac{2\beta}{Z^2}\left(1 - \frac{Z^2}{\beta}\right) + \frac{2\beta}{Z^2}\left[1 - \frac{Z^2}{\beta}\right]^{1/2}. \tag{2.12}$$

The other one is from the fact that the Z^2 is the coefficient of the radion kinetic term after undoing the kinetic mixing. It is therefore required to be positive ($Z^2 > 0$) in order to keep the radion kinetic term definitely positive, i.e.

$$-\frac{1}{12}\left(1 + \sqrt{1 + \frac{4}{\gamma^2}}\right) < \xi < \frac{1}{12}\left(\sqrt{1 + \frac{4}{\gamma^2}} - 1\right). \tag{2.13}$$

We now discuss the previous estimations on the radion mass and some model parameters. All phenomenological signatures of the RS model including the radion - Higgs mixing are specified by five parameters

$$\Lambda_\phi,\ \frac{m_0}{M_{\rm Pl}},\ m_h,\ m_\phi,\ \xi. \tag{2.14}$$

For the reliability of the RS solution, the ratio $\frac{m_0}{M_{\rm Pl}}$ is usually taken around $0.01 \leq \frac{m_0}{M_{\rm Pl}} \leq 0.1$ to avoid too large bulk curvature [25]. Therefore, we consider the case of $\Lambda_\phi = 5$ TeV and $\frac{m_0}{M_{\rm Pl}} = 0.1$, where the effect of radion on the oblique parameters is small [26]. The radion mass in the RS model is expected to be light as by one of the simplest stabilization mechanisms predicted in range of $10 - 100$ GeV [4]. We choose $\xi = 0, \pm 1/6$, which are in agrement with those in Ref. [6] with $\xi\gamma \ll 1, Z^2 \approx 1$.

The recent results in Refs. [23, 27] have shown that the radion can be naturally stabilized with a smaller mass, for example, in order of 10^{-2} GeV. Perhaps a much lower mass can also be accommodated with little fine-tuning, which is necessary for the conversion processes considered below to be more relevant, but in general the radion is not naturally such small. There is nothing wrong with finding that the experiments do not yet probe the theoretically expected parameter space of the certain models, but that it comes close, and therefore it may be worth looking for the radion in this way. In this work, we will show the cross-section expressions for the general cases with arbitrary radion mass, but the numerical treatments only take the GeV radions into account where the effect of Higgs-radion mixing may become important. (Let us recall that in the large extradimensions, the radion is typically very light, with mass between 10^{-3} eV and MeV.)

3. Radion coupling to photons

For the massless gauge bosons such as photon and gluon, there are no large couplings to the radion because there are no brane-localized mass terms. However, the potentially large contributions to these couplings may come from the loop effects of the gauge bosons, the higgs field and the top quark as well as the localized trace anomalies (there are also the bulk contributions if the massless gauge bosons are set off-brane, but this does not change the main results of the paper) [6, 7, 9, 28].

Referring the reader for details of the radion-photon coupling to Ref. [6, 7], we lay out the necessary radion-photon coupling

$$\mathcal{L}_{\gamma\gamma\phi} = \frac{1}{2} c_{\phi\gamma\gamma} \phi F_{\mu\nu} F^{\mu\nu}, \tag{3.1}$$

with

$$c_{\phi\gamma\gamma} = -\frac{\alpha}{4\pi\Lambda_\phi} \left\{ a(b_2 + b_Y) - a_{12}[F_1(\tau_W) + 4/3 F_{1/2}(\tau_t)] \right\}, \tag{3.2}$$

where $b_2 = 19/6, b_Y = -41/6$ are the $\mathrm{SU}(2)_L \otimes \mathrm{U}(1)_Y$ β-function coefficients in the SM, and $a_{12} = a + c/\gamma$, $\tau_t = 4m_t^2/q^2$ and $\tau_W = 4m_W^2/q^2$.

The form factors $F_{1/2}(\tau_t)$ and $F_1(\tau_W)$ are given by

$$\begin{aligned} F_{1/2}(\tau) &= -2\tau[1 + (1-\tau) f(\tau)], \\ F_1(\tau) &= 2 + 3\tau + 3\tau(2-\tau) f(\tau), \end{aligned} \tag{3.3}$$

with

$$f(\tau) = \begin{cases} \arcsin^2(1/\sqrt{\tau}), & \tau \geq 1, \\ -\frac{1}{4}\left[\ln\left(\frac{1+\sqrt{1-\tau}}{1-\sqrt{1-\tau}} \right) - i\pi \right]^2 & \tau < 1. \end{cases} \tag{3.4}$$

The important property of $F_{1/2}(\tau)$ is that, for $\tau > 1$, it very quickly saturates to $-4/3$, and to 0 for $\tau < 1$. $F_1(\tau)$ saturates quickly to 7 for $\tau > 1$, and to 0 for $\tau < 1$ [9].

Now let us turn to our main interest, i.e., the photon conversions into radions in the external EM fields.

4. Photon-to-radion conversions

The photon regeneration experiment, using RF photons, was described in Ref. [29]. That experiment consists of two cavities which are placed a small distance apart. A more or less homogeneous magnetic field exists in both the cavities. The first, or emitting cavity, is excited by incoming RF radiation. Depending on the radion-photon coupling constant, a certain amount of RF energy will be deposed in the second, or receiving cavity. Using Feynman diagram technique we have considered the conversion of the photon into axions in external EM field [19]. In this paper, in the framework of the RS model we apply this method to reconsider the conversion of photon into the radion.

Let us consider the conversion of the photon γ with momentum q into radion ϕ with momentum p in an external EM field. Using the Feynman rules we get the following expression for the matrix element

$$< p|M_\phi|q >= \frac{c_{\phi\gamma\gamma}}{(2\pi)^2\sqrt{p_0 q_0}}\varepsilon^\mu(\mathbf{q},\lambda)q^\nu \int_V e^{i\mathbf{kr}}F^{\rm class}_{\nu\mu}d\mathbf{r}, \tag{4.1}$$

where $\mathbf{k}\equiv\mathbf{p}-\mathbf{q}$ and $\varepsilon^\mu(\mathbf{q},\lambda)$ represents the polarization vector of the photon. Expression (4.1) is valid for an arbitrary external EM field. In the following we shall use it for the cases, namely in the electric field of a flat condenser, in the static magnetic field of a solenoid and in a wave guide with the TE_{10} mode. Here we use the following notations: $q\equiv|\mathbf{q}|$, $p\equiv|\mathbf{p}|=(q^2-m_\phi^2)^{1/2}$ and θ is the angle between $\mathbf{p}$ and $\mathbf{q}$.

4.1 Conversion in electric field

Let us take the EM field as a homogeneous electric field of a flat condenser of size $l_x\times l_y\times l_z$. We shall use the coordinate system with the x axis parallel to the direction of the field, i.e., $F^{01}=-F^{10}=E$. Then the matrix element is given by

$$< p|M_\phi|q >= \frac{c_{\phi\gamma\gamma}}{(2\pi)^2\sqrt{p_0 q_0}}\varepsilon^1(\mathbf{q},\lambda)q^0 F_e(\mathbf{k}), \tag{4.2}$$

where

$$F_e(\mathbf{k}) = \int_V e^{i\mathbf{kr}}E(\mathbf{r})d\mathbf{r} \tag{4.3}$$

For a homogeneous electric field of intensity E we have

$$F_e(\mathbf{k}) = 8E\sin(l_x k_x/2)\sin(l_y k_y/2)\sin(l_z k_z/2)(k_x k_y k_z)^{-1}. \tag{4.4}$$

Squaring the matrix element (4.2) we obtain

$$\frac{d\sigma^e(\gamma\to\phi)}{d\Omega} = \frac{8c^2_{\phi\gamma\gamma}E^2q^2}{\pi^2}\left[\frac{\sin(\frac{1}{2}l_x k_x)\sin(\frac{1}{2}l_y k_y)\sin(\frac{1}{2}l_z k_z)}{k_x k_y k_z}\right]^2\left(1-\frac{q_x^2}{q^2}\right). \tag{4.5}$$

From Eq.(4.5) we see that if the photon moves in the direction of the electric field, i.e., $q^\mu=(q,q,0,0)$, the differential cross-section vanishes.

We shall explore the following case: The momentum of photon is parallel to the z axis, i.e., $q^\mu=(q,0,0,q)$. In the spherical coordinates we then have

$$p_x = p\sin\theta\cos\varphi,\qquad p_y = p\sin\theta\sin\varphi,\qquad p_z = p\cos\theta, \tag{4.6}$$

where φ is the angle between the x axis and the projection of $\mathbf{p}$ on the xy plane. Substitution of Eq.(4.6) into Eq.(4.5) yields

$$\begin{aligned}\frac{d\sigma^e(\gamma\to\phi)}{d\Omega} &= \frac{8c^2_{\phi\gamma\gamma}E^2q^2}{\pi^2}\left[\sin\frac{l_x p\sin\theta\cos\varphi}{2}\sin\frac{l_y p\sin\theta\sin\varphi}{2}\sin\frac{l_z(q-p\cos\theta)}{2}\right]^2\\ &\times\ [p^2(q-p\cos\theta)\sin^2\theta\cos\varphi\sin\varphi]^{-2}.\end{aligned} \tag{4.7}$$

Let us evaluate the differential cross-section in the following several limits. When the scattering angle θ is very small, i.e., $\sin\theta \approx \theta$, we get then

$$\frac{d\sigma^e(\gamma \to \phi)}{d\Omega} = \frac{c^2_{\phi\gamma\gamma} E^2 l_x^2 l_y^2}{2\pi^2 \left(1 - \sqrt{1 - \frac{m_\phi^2}{q^2}}\right)^2} \sin^2 \left[\frac{l_z q}{2}\left(1 - \sqrt{1 - \frac{m_\phi^2}{q^2}}\right)\right]. \tag{4.8}$$

In the limit $\theta \to \frac{\pi}{2}$ and $\varphi \to 0$, the differential cross-section (4.7) becomes

$$\frac{d\sigma^e(\gamma \to \phi)}{d\Omega} = \frac{2c^2_{\phi\gamma\gamma} E^2 l_y^2}{\pi^2(q^2 - m_\phi^2)} \sin^2 \frac{l_x q\sqrt{1 - \frac{m_\phi^2}{q^2}}}{2} \sin^2 \frac{l_z q}{2}. \tag{4.9}$$

When $\theta \to \frac{\pi}{2}$ and $\varphi \to \frac{\pi}{2}$, Eq.(4.7) gives

$$\frac{d\sigma^e(\gamma \to \phi)}{d\Omega} = \frac{2c^2_{\phi\gamma\gamma} E^2 l_x^2}{\pi^2(q^2 - m_\phi^2)} \sin^2 \frac{l_y q\sqrt{1 - \frac{m_\phi^2}{q^2}}}{2} \sin^2 \frac{l_z q}{2}, \tag{4.10}$$

which is similar to Eq.(4.9) with $l_x \leftrightarrows l_y$.

From Eqs.(4.8,4.9,4.10) we see that the differential cross-sections in the direction of the condenser depends quadratically on the intensity E, the sizes of condenser, and the photon momentum q. Since the external EM field is classical we can therefore increase the scattering probability as much as possible by increasing the intensity of the field and/or the condenser volume containing the field.

Now we are interested in the total cross-section $\sigma^e(q) = \int d\Omega(d\sigma^e/d\Omega)$. Since the integrand as given by the general formula (4.7) does not simultaneously vanish over the integrated domain, the total cross-section is always different from (i.e. larger than) zero. Because the integrand as well as the total cross-section which depend on provided photon high momentum q (at least larger than the radion mass) are very rapidly oscillated with q (an evaluation for $l_{x,y,z}q$ from the values given below implies this), the numerical treatments are actually issued by the following problems:

1. A plot constructed from a finite number of points where the neighboring ones (point next to point) are connected by a line would not have an obvious variation rule. In principle it is an arbitrary line, not reflecting the realistic variation of the cross-section or the spectrum.

2. An average cross-section, $\bar{\sigma}^e(\bar{q}) = \frac{1}{q_2 - q_1}\int_{q_1}^{q_2} dq\sigma^e(q)$, also changes arbitrarily due to the current numerical methods calculating the integral with a finite number of divisional points in the integrated domain.

To overcome these difficulties, we will plot a large spectrum of point $(q, \sigma^e(q))$ corresponding to a large number of values of q in the interested domain. The orientation of the spectrum will reflect the correct variation of the cross-section. Let us note that the resulting cross-section will be almost independent of the radion mass values if $m_\phi^2/q^2 \ll 1$.

In practice, to evaluate the total cross-section for Eq.(4.7), the parameters are chosen as follows: $\Lambda_\phi = 5$ TeV, $\xi = 0, \pm 1/6, \alpha = 1/128$, $l_x = l_y = l_z = 1$ m $= 5.07 \times 10^6$ eV^{-1}, $E = 100$ KV/m $= 6.517 \times 10^{-2}$ eV^2 [19], and the radion mass can be taken in the limit $m_\phi = 10$ GeV [23]. The total cross-section on the selected range of momenta q for the radion production are given in Figure 1. Here the different values $\xi = 0, \pm 1/6$ approximately yield the same contribution to the cross-section. As demonstrated in the two plots, when the number of points is increased the resonances become shapely. We can see from Figure 1 that the cross-section is quite small to be measurable because of the current experimental limits, even though the resonances presented in this case.

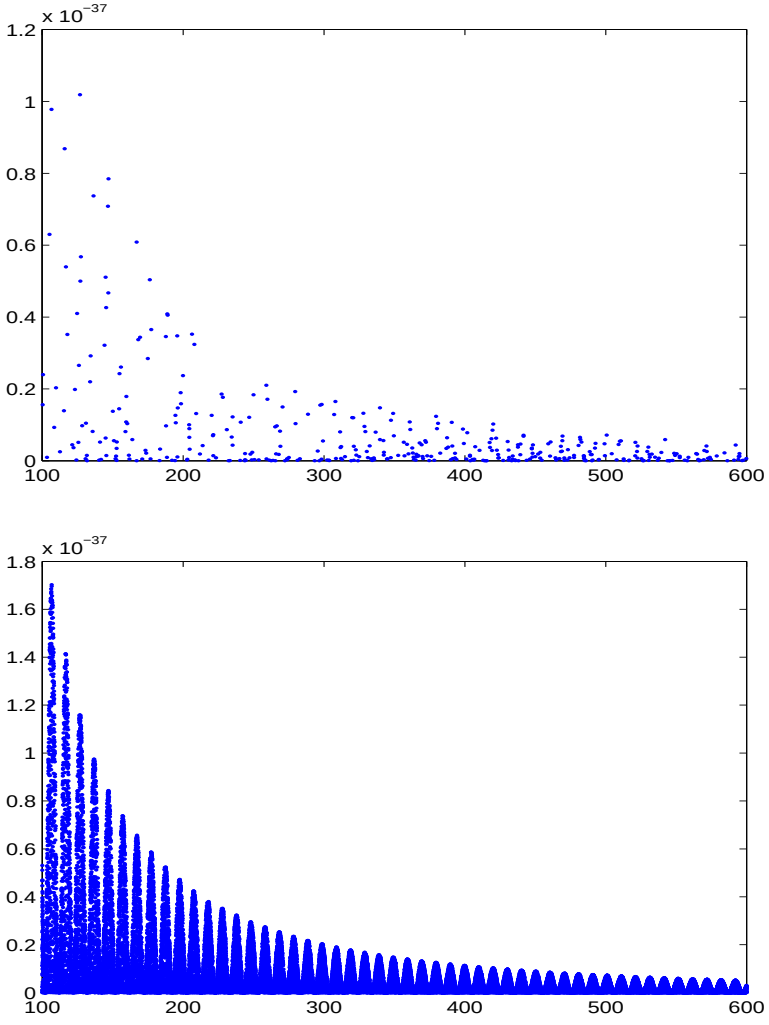

Figure 1: The total cross-section (cm^2) for conversion in electric field as a function of provided momentum $q = 100 - 600$ GeV. The upper plot is depicted as 400 points, and the lower one is for 30000 points.

In addition, it follows from Figure 1 that the changing of the cross-section in the domain

100 GeV $< q < q_t$ GeV is much faster than the remaining domain $q > q_t$ GeV, where the "transition point" q_t is around on $200 - 300$ GeV. In the second one, the cross-section approaches constant when q is large. The reason for this is that the total scattering cross-section is dominated by forward scattering at large q. This can be seen in the three subcases of Eqs. (4.8,4.9,4.10). Up to rapidly oscillating (and bounded) terms, the latter two behave like $1/q^2$, whereas the first one is essentially q-independent in this limit (averaging over oscillations). This can be seen directly also from the term in square brackets in Eq. (4.5). Due to the chosen geometry, k_x and k_y are always large ($\sim q$), but k_z can be small for forward scattering, and thus $\sin k_z/k_z \to 1$.

The slope of the cross-section with the large q can be approximated as $\sigma'(q) \simeq 4.142 \times 10^{-61}$ cm^3, which may be seen from the Figure 1. This value justifies again that the cross-section tends to the constant. The transition point q_t can be naively evaluated as intersection of the asymptote of the cross-section in the large q domain and the horizontal axis, that is $q_t \simeq q - \frac{\sigma(q)}{\sigma'(q)} \simeq 230$ GeV (valid for large q). It is noticed that this parameter is the derivative one, not concerning as any characteristic scales of the model. Its value depends only on a choice of the parameters such as the radion mass, the size of condenser, the field strength, and so on.

Let us remark that when the momentum of photon is perpendicular to the electric field E we have then the most optimal condition for the experiments.

4.2 Conversion in magnetic field

Next, we consider the conversion of photon into radion in a homogeneous magnetic field of the solenoid with radius R and a length l. Without loss of generality we suppose that the direction of the magnetic field is parallel to the z-axis, i.e., $F^{12} = -F^{21} = B$. The matrix element is given then

$$< p \mid M \mid q >= \frac{c_{\phi\gamma\gamma}}{(2\pi)^2\sqrt{p_0 q_0}}(\varepsilon^2(\mathbf{q},\sigma)q^1 - \varepsilon^1(\mathbf{q},\sigma)q^2)F_m(\mathbf{k}), \tag{4.11}$$

where

$$F_m(\mathbf{k}) = \int_V e^{i\mathbf{kr}}B(\mathbf{r})d\mathbf{r}. \tag{4.12}$$

In the cylindrical coordinates, the integral (4.11) becomes

$$F_m(\mathbf{k}) = B\int_0^R \varrho d\varrho \int_0^{2\pi} \exp\{i[k_x\cos\varphi + k_y \sin\varphi]\}d\varphi \int_{-l/2}^{l/2} \exp\{ik_z z\}dz. \tag{4.13}$$

After some manipulations we get

$$F_m(\mathbf{k}) = \frac{4\pi BR}{k_z\sqrt{k_x^2+k_y^2}} j_1\left(R\sqrt{k_x^2+k_y^2}\right)\sin\left(\frac{lk_z}{2}\right), \tag{4.14}$$

where j_1 is the spherical Bessel function of the first kind.

From Eqs.(4.11,4.14) we obtain the differential cross-section as follows

$$\frac{d\sigma^m(\gamma\to\phi)}{d\Omega'} = \frac{2c_{\phi\gamma\gamma}^2 R^2B^2}{k_z^2(k_x^2+k_y^2)} j_1^2\left(R\sqrt{k_x^2+k_y^2}\right)\sin^2\left(\frac{lk_z}{2}\right)(q_x-q_y)^2. \tag{4.15}$$

Eq.(4.15) shows that when the momentum of the photon is parallel to the z-axis (the direction of the magnetic field), the differential cross-section vanishes. This result is the same as the previous section. It implies that if the momentum of the photon is parallel to the EM field, then there is no conversion. If the momentum of the photon is parallel to the x-axis, i.e., $q^\mu = (q, q, 0, 0)$, then Eq.(4.15) gets the form

$$\frac{d\sigma^m(\gamma \to \phi)}{d\Omega'} = \frac{2c_{\phi\gamma\gamma}^2 R^2 B^2 q^2 j_1^2 \left(R\sqrt{(q - p\cos\theta)^2 + (p\sin\theta\cos\varphi')^2}\right)}{(p\sin\theta\sin\varphi')^2[(q - p\cos\theta)^2 + (p\sin\theta\cos\varphi')^2]} \times \sin^2\left(\frac{lp}{2}\sin\theta\sin\varphi'\right), \tag{4.16}$$

where φ' is the angle between the y-axis and the projection of $\mathbf{p}$ on the yz-plane [9].

Now we are interested in several cases. The first case is for $\theta \approx 0$ we have

$$\frac{d\sigma^m(\gamma \to \phi)}{d\Omega'} = \frac{c_{\phi\gamma\gamma}^2 R^2 B^2 l^2 j_1^2 \left[Rq(1 - \sqrt{1 - \frac{m_\phi^2}{q^2}})\right]}{2\left(1 - \sqrt{1 - \frac{m_\phi^2}{q^2}}\right)^2}. \tag{4.17}$$

In the limit $\theta \to \pi/2$ and $\varphi' \to 0$, Eq.(4.16) becomes

$$\frac{d\sigma^m(\gamma \to \phi)}{d\Omega'} = \frac{c_{\phi\gamma\gamma}^2 R^2 l^2 B^2 q^2}{2(2q^2 - m_\phi^2)} j_1^2\left(R\sqrt{2q^2 - m_\phi^2}\right). \tag{4.18}$$

For the last case, the limit $\theta \to \pi/2, \varphi' \to \pi/2$ yields

$$\frac{d\sigma^m(\gamma \to \phi)}{d\Omega'} = \frac{2c_{\phi\gamma\gamma}^2 R^2 B^2}{(q^2 - m_\phi^2)} j_1^2(Rq)\sin^2\left(\frac{lq\sqrt{1 - \frac{m_\phi^2}{q^2}}}{2}\right). \tag{4.19}$$

To evaluate the total cross-section from the general formula (4.16), the parameter values for Λ_ϕ, α and m_ϕ are given as before. The remaining ones are chosen as follows: $R = l = 1$ m $= 5.07 \times 10^6$ eV^{-1} and $B = 9$ Tesla $= 9 \times 195.35$ eV^2 [21]. The total cross-section on the selected range of momenta q by Eq.(4.16) for three cases $\xi = 0, \pm\frac{1}{6}$ yields the same value which is presented as in Figure 2.

From Fig. 2 we see that the total cross-section for the radion production in the magnetic field are much bigger than that of the electric field. This happens because of $B \gg E$. In this case, the resonant figure disappears although the number of points is much increased. This may be due to the fact that the cross-section is given as an incoherent multiple of the Bessel and trigonometric functions. Notice also that in similarity to the previous case, the behavior of the cross-section is different in the two domains divided by a transition point around on $200 - 300$ GeV. It is worth mentioning here if the radion mass is much smaller than the provided photon momentum, the cross-sections are much larger.

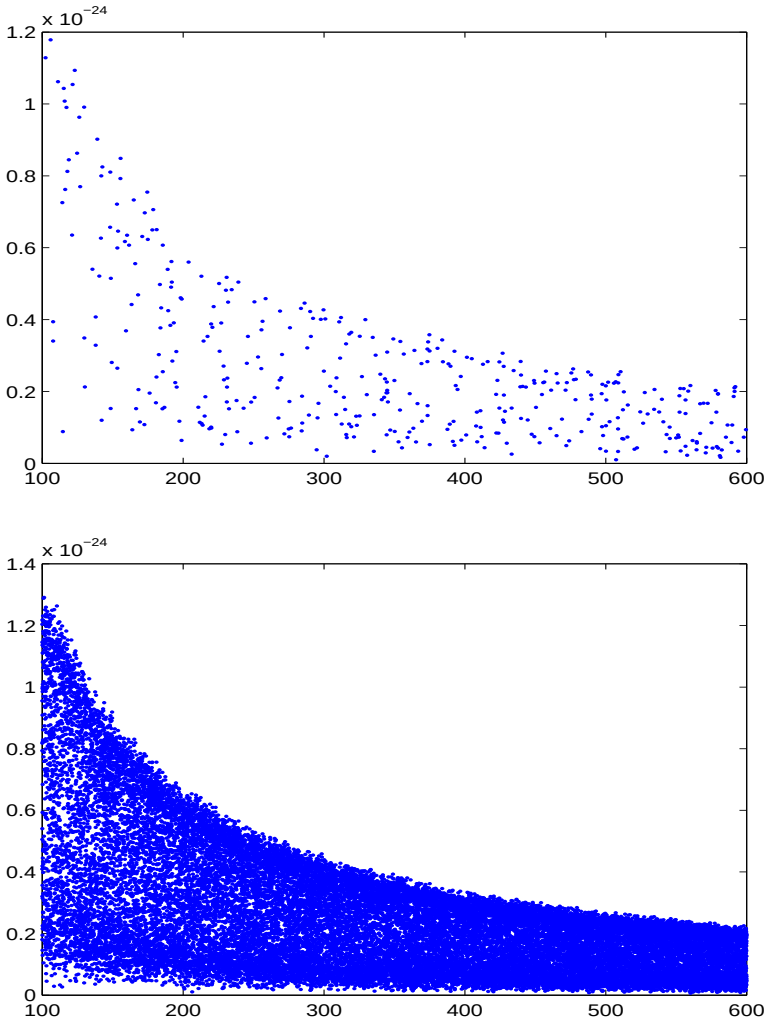

Figure 2: The total cross-section (cm^2) for conversion in magnetic field as a function of provided momentum $q = 100 - 600$ GeV. The upper plot is depicted as 400 points, and the lower one is for 30000 points.

4.3 Conversion in wave guide

We will show that the cross-section can also be enhanced in comparison to the electric field case when the conversion exists in a varying EM field. Let us consider a case of the periodic external EM field of the wave guide with the TE_{10} mode. The nontrivial solution of this mode is given by [30]

$$H_z = H_o \cos\left(\frac{\pi x}{l_x}\right) e^{ikz - i\omega t},$$
$$H_x = -\frac{ikl_x}{\pi} H_o \sin\left(\frac{\pi x}{l_x}\right) e^{ikz - i\omega t},$$

$$E_y = i\frac{\omega l_x}{\pi} H_o \sin\left(\frac{\pi x}{l_x}\right) e^{ikz-i\omega t}, \tag{4.20}$$

with the cutoff frequency $\omega_o = \frac{\pi}{l_x}$.

The expression for the matrix element is

$$\begin{aligned}\langle p|\mathcal{M}|q\rangle = & \frac{c_{\phi\gamma\gamma}}{(2\pi)^2\sqrt{p_0 q_0}} \left\{\varepsilon_2(\mathbf{q},\tau)q_0 F_y + \left[\varepsilon_2(\mathbf{q},\tau)q_3 - \varepsilon_3(\mathbf{q},\tau)q_2\right] F_x \right. \\ & \left. + \left[\varepsilon_1(\mathbf{q},\tau)q_2 - \varepsilon_2(\mathbf{q},\tau)q_1\right] F_z \right\}, \end{aligned} \tag{4.21}$$

where $p_0 \equiv q_0 + \omega$, and

$$\begin{aligned} F_x &= -\frac{8kl_x H_0 (q_x - p_x)\cos[\frac{1}{2}l_x(q_x-p_x)]\sin[\frac{1}{2}l_y(q_y-p_y)]\sin[\frac{1}{2}l_z(q_z-p_z+k)]}{\pi[(q_x-p_x)^2 - \frac{\pi^2}{l_x^2}](q_y-p_y)(q_z-p_z+k)}, \\ F_y &= -F_x, \\ F_z &= -\frac{8\pi H_0 \cos[\frac{1}{2}l_x(q_x-p_x)]\sin[\frac{1}{2}l_y(q_y-p_y)]\sin[\frac{1}{2}l_z(q_z-p_z+k)]}{l_x[(q_x-p_x)^2 - \frac{\pi^2}{l_x^2}](q_y-p_y)(q_z-p_z+k)}. \end{aligned} \tag{4.22}$$

Substituting Eq.(4.22) into Eq.(4.21) we obtain the differential cross-section

$$\begin{aligned}\frac{d\sigma(\gamma\to\phi)}{d\Omega} = & \frac{c_{\phi\gamma\gamma}^2 p_o}{2(2\pi)^2 q_0}\left[({q_0}^2 - {q_y}^2){F_y}^2 + 2q_0[(q_z-q_y)F_x + (q_y-q_x)F_z]F_y + (q_y-q_z)^2{F_x}^2\right. \\ & \left. + 2[(q_z-q_y)q_y + (q_y-q_z)q_x]F_xF_z + (q_x-q_y)^2{F_z}^2\right]. \end{aligned} \tag{4.23}$$

When the momentum of the photon is parallel to the z - axis, the differential cross-section vanishes. This is the same as in the static EM fields. If the momentum of the photon is parallel to the x - axis, Eq.(4.23) becomes

$$\begin{aligned}\frac{d\sigma(\gamma\to\phi)}{d\Omega} = & \frac{8c_{\phi\gamma\gamma}^2 H_0^2 l_x^2 q^2}{\pi^4}\left[\cos\frac{l_x(q-p\cos\theta)}{2}\sin\frac{l_y p\sin\theta\cos\varphi}{2}\sin\frac{l_z(p\sin\theta\sin\varphi+k)}{2}\right]^2 \\ & \times\left(1+\frac{\omega}{q}\right)\left[\omega(q-p\cos\theta)+\frac{\pi^2}{l_x^2}\right]^2\left[(q-p\cos\theta)^2-\frac{\pi^2}{l_x^2}\right]^{-2} \\ & \times\left[(p\sin\theta\cos\varphi)\,(p\sin\theta\sin\varphi+k)\right]^{-2}, \end{aligned} \tag{4.24}$$

where $p = \sqrt{(q+\omega)^2 - m_\phi^2}$.

To compare the cross-section with the previous cases, we take $H_0 = B$, $q = 500$ GeV and $m_\phi = 10$ GeV, for example, into account. The remaining parameters are chosen as before. In Fig. 3 we plot the total cross-section as a function of the high frequency external source: $\omega/\omega_0 = 5000 - 10000$. The cross-section as presented is on average much larger than that of the static electric field, but smaller than that of the static magnetic field. It can become comparable to the latter when the frequency is large enough. When the number of points plotted is increased, the shape of steps become obvious. But, what do the steps mean?

Let us first note that in this case the total cross-section increases because it is proportional to ω^2 as can be evaluated from (4.24) due to $\omega_0 \ll \omega, k \ll m_\phi \ll p, q$. Since the

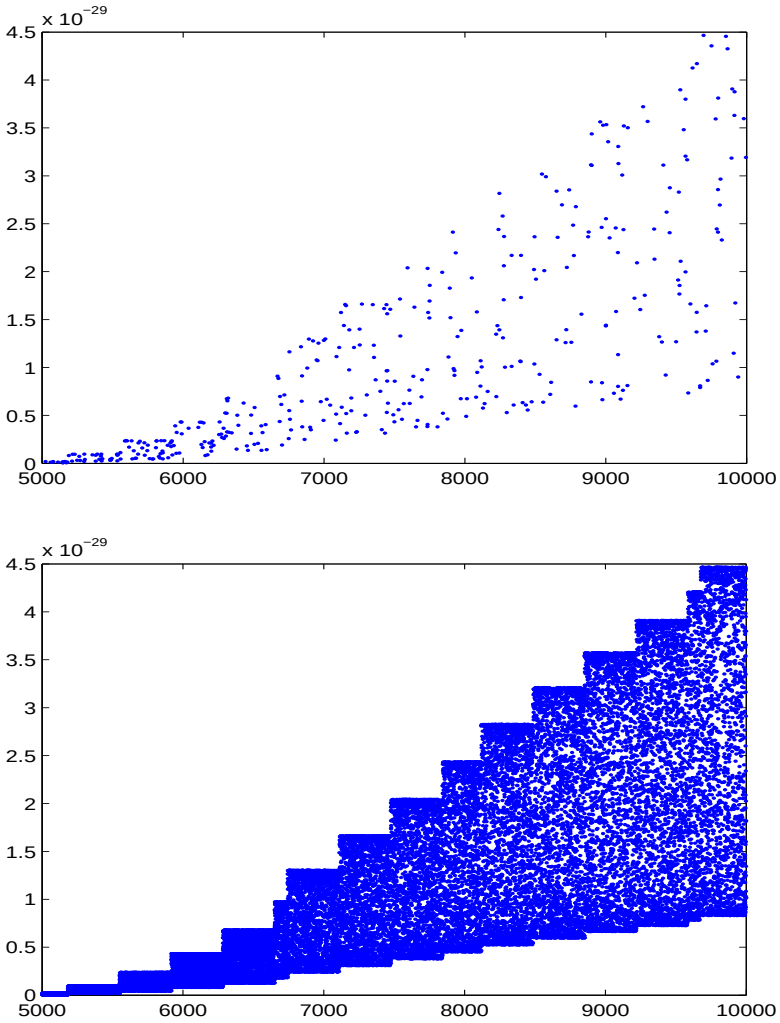

Figure 3: The total cross-section (cm^2) as a function of the external field frequency $\omega/\omega_0 = 5000 - 10000$ corresponding to the value $q = 500$ GeV. The upper plot is depicted as 400 points, and the lower one is for 30000 points.

provided photon source is fixed as mentioned, any enhancement in the external EM field is correspondingly used to convert into possible additionally-produced radions, which depends drastically on the increasing rate and amount of the external field energy momentum $(\omega, \mathbf{k})$. The scale for this energy momentum is proportional to $k = |\mathbf{k}| \simeq \omega \sim 10^3\omega_0 \sim 10^{-3}$ eV, which is so small in comparison to the radion mass. To create such a heavy radion, $m_\phi = 10$ GeV $\gg 10^{-3}$ eV, an appropriate change in (namely, a large enough amount of) ω could be needed while the cross-section is still remained constant. And, when the ω approaches the upper bound of this amount, the radion is just generated and the cross-section is then stepped as seen in the plot. This happens similarly for the next levels. Notice also that, in principle, this case could be observed experimentally since one can control the

frequency ω.

Let us remind that the cutoff frequency of the TE_{10} is $\omega_0 = \frac{\pi}{l_x}$ and at any given frequency ω only a finite number of modes can propagate [30]. It is often convenient to choose the dimensions of the guide such that in the operating frequency, only the lowest mode can occur. This is an important point in order to apply it in experiments.

5. Conclusion

With the help of the coupling of radion to photons, we have obtained the conversion cross-sections of photon into radion in the presence of several external fields such as the static electric field of the condenser, the static magnetic field of the solenoid and the periodic electromagnetic field of the wave guide. The numerical evaluations of the total cross-sections are also given.

The production cross-sections of radion in the static electric field is quite small, which is not expected to be easily observed. However, the cross-section in the static magnetic and periodic electromagnetic fields are much enhanced, which can be measurable in the present experiments.

Let us mention again that since the Randall-Sundrum model radion is quite heavy with masses at least in the GeV range, the experiments are only available if the provided photon sources are in high energies, as we often take some hundreds of GeV. Also, the light radions in the model if they really exist are favored in these experiments.

The original experiments were designed for searching axions and gravitons which are the very light particles. Such possible light radions if exiting in the model would be more accessible. In this case, one can use our general formulae of the cross-sections, then by the same procedure one can achieve the results, which have not yet displayed in this work.

In this work we have considered only a theoretical basis for the experiments, other techniques concerning construction and particle detection can be found in Ref. [21]. It is emphasized that our study can be applied for searching the possible light radions in other models such as the large extradimensions.

Acknowledgments

We would like to thank the referees for their critical remarks/comments which amended a lot the article. The work was supported in part by National Foundation for Science and Technology Development (NAFOSTED) of Vietnam.

References

[1] N. Arkani-Hamed, S. Dimopoulos and G. Dvali, *The hierarchy problem and new dimensions at a millimeter, Phys. Lett.* **B429**, 263 (1998).

[2] L. Randall and R. Sundrum, *A large mass hierarchy from a small extra dimension, Phys. Rev. Lett.* **83**, 3370 (1999).

[3] C. Csaki, M. Graesser, L. Randall, and J.Terning, *Cosmology of brane modes with radion stabilization, Phys.Rev.***D 62**, 045015 (2000).

[4] See, for example, W. D. Goldberger and M. B. Wise, *Modulus stabilization with bulk fields, Phys. Rev. Lett.* **83**, 4922 (1999);
Phenomenology of a stabilized modulus, Phys. Lett. **B 475**, 275 (2000).

[5] U. Mahanta and A. Datta, *Production of light stabilized radion at high-energy hadron collider, Phys. Lett.* **B 483**, 196 (2000).

[6] G. F. Giudice, R. Rattazzi and J. D. Wells, *Graviscalars from higher dimensional metrics and curvature Higgs mixing, Nucl. Phys.* **B 595**, 250 (2001).

[7] M. Chaichian, A. Datta, K. Huitu, and Z. Yu, *Radion and Higgs mixing at the LHC, Phys. Lett.* **B 524**, 161 (2002).

[8] D. Dominici, B. Grzadkowski, J. F. Gunion and M. Toharia, *The Scalar sector of the Randall-Sundrum model, Nucl. Phys.* **B 671**, 243 (2003).

[9] C. Csaki, J. Hubisz and S. J. Lee, *Radion phenomenology in realistic warped space models, Phys. Rev.* **D 76**, 125015 (2007).

[10] J. Bagger and M. Redi, *Radion effective theory in the detuned Randall-Sundrum model, J. High Energy Phys.* **04**, 031 (2004).

[11] V.P.Goncalves and W.K. Sauter, *Radion production in exclusive processes at CERN LHC*, *Phys.Rev.* **D 82**, 056009 (2010).

[12] Hooman Davoudiasl, Thomas McElmurry, and Amarjit Soni, *Precocious Diphoton Signals of the Little Radion at Hadron Colliders Phys.Rev.* **D 82**, 115028 (2010).

[13] H. Primakoff, *Photo-Production of Neutral Mesons in Nuclear Electric Fields and the Mean Life of the Neutral Meson, Phys. Rev.* **81**, 899 (1951).

[14] P. Sikivie, *Detection rates for "invisible"-axion searches, Phys. Rev.* **D 32**, 2988 (1985).

[15] A. K. Ganguly, *Pseudoscalar photon mixing in a magnetized medium, Annals Phys.* **321**, 1457 (2006);
A. Mirizzi, G. G. Raffelt and'P. D. Serpico, *Signatures of axion-like particles in the spectra of TeV gamma-ray sources, Phys. Rev.* **D 76**, 023001 (2007);
N. Agarwal, P. Jain, D. W. Mc.Kay and J. P. Ralston, *Signatures of Pseudoscalar Photon Mixing in CMB Radiation, Phys. Rev.* **D 78**, 085028 (2008).

[16] S. Andriamonje *et al., An Improved limit on the axion-photon coupling from the CAST experiment, JCAP* **0704**, 010 (2007);
E. Zavattini *al., New PVLAS results and limits on magnetically induced optical rotation and ellipticity in vacuum, Phys. Rev.* **D 77**, 032006 (2008);
A. Rubbia and A. S. Sakharov, *Constraining axion by polarized prompt emission from gamma ray bursts, Astropart. Phys.* **29**, 20 (2008).

[17] H. N. Long and L. K. Huong, *Photoproduction of gravitons and dilatons in an external electromagnetic field, Mod. Phys. Lett.* **A 6**, 2315 (1991);
D. V. Soa and H. N. Long, *Photoproduction of dilatons in an external magnetic field, Mod. Phys. Lett.* **A 15**, 23 (2000).

[18] H.N. Long, D. V. Soa and T. A. Tuan, *The conversion of gravitons into photons in a periodic external electromagnetic field, Phys. Lett.* **A 186**, 382 (1994).

[19] H. N. Long, D. V. Soa and Tuan A. Tran, *Electromagnetic detection of axions, Phys. Lett.* **B 357**, 469 (1995).

[20] I. F. Ginzburg *et al., Colliding gamma e and gamma gamma Beams Based on the Single Pass Accelerators (of Vlepp Type), Nucl. Instr. and Meth* **205**, 47 (1983);
V. I. Telnov, *Status of gamma-gamma, gamma-electron colliders, Nucl. Phys. Proc. Suppl.* **82** (2000) 359.

[21] S. Andriamonie *et al., The CERN Axion Solar Telescope (CAST): An update, Nucl. Phys. Proc. Suppl.* **138**, 41 (2005);
An Improved limit on the axion-photon coupling from the CAST experiment, JCAP **0704**, 010 (2007).

[22] S. Bae, P. Ko, H. S. Lee, and J. Lee, *Phenomenology of the radion in Randall - Sundrum scenario at colliders, Phys. Lett.* **B 487**, 299 (2000).

[23] C. Csaki, M. L. Graesser and G. D. Kribs, *Radion dynamics and electroweak physics, Phys. Rev.* **D 63**, 065002 (2001);
H. Davoudiasl and E. Ponton, *B-Decay Signatures of Warped Top - Condensation, Phys. Lett.* **B 680**, 247 (2009);
Yang Bai, Marcela Carena, and Eduardo Pronton, *The Planck Scale from Top Condensation, Phys. Rev.* **D 81**, 065004(2010).

[24] K. Cheung *et al., Probing the radion-Higgs mixing at hadronic colliders, Phys. Rev.* **D 69**, 075011 (2004).

[25] H. Davoudiasl, J. L. Hewett, and T. G. Rizzo, *Experimental probes of localized gravity: On and off the wall, Phys. Rev.* **D 63**, 075004 (2001).

[26] C. S. Kim, J. D. Kim and Jeong-hyeon Song, *Top quark Kaluza-Klein mode mixing in the Randall-Sundrum bulk standard model and* $B \to Xs\gamma$, *Phys. Rev.* **D 67**, 015001 (2003).

[27] A. Wang and N. O. Santos, *The hearachy problem, Radion mass, Localization of gravity and 4D effective Newtonian potential in string theory on* Z^1/Z_2, *Int. J. Mod. Phys.* **A25**, 1661(2010).

[28] M. S. Carena, E. Ponton, T. M. P. Tait and C. E. M. Wagner, *Opaque branes in warped backgrounds, Phys. Rev.* **D 67**, 096006 (2003).

[29] F. Hoogeveen, *Terrestrial axion production and detection using RF cavities, Phys. Lett.* **B 288**, 195 (1992).

[30] J. D. Jackson, *Classical Electrodynamic,* Wiley, New York 1975, section 8.4, p.274.